

# On the ionisation fraction in protoplanetary disks III. The effect of X-ray flares on gas-phase chemistry

Martin Ilgner and Richard P. Nelson

Astronomy Unit, Queen Mary, Mile End Road, London E1 4NS, U.K.  
e-mail: M.Ilgner@qmul.ac.uk, R.P.Nelson@qmul.ac.uk

Received 29 March 2006 / Accepted 11 May 2006

## ABSTRACT

**Context.** Recent observations of the X-ray emission from T Tauri stars in the Orion nebula have shown that they undergo frequent outbursts in their X-ray luminosity. These X-ray flares are characterised by increases in luminosity by two orders of magnitude, a typical duration of less than one day, and a significant hardening of the X-ray spectrum.

**Aims.** It is unknown what effect these X-ray flares will have on the ionisation fraction and dead-zone structure in protoplanetary disks. We present the results of calculations designed to address this question.

**Methods.** We have performed calculations of the ionisation fraction in a standard  $\alpha$ -disk model using two different chemical reaction networks. We include in our models ionisation due to X-rays from the central star, and calculate the time-dependent ionisation fraction and dead-zone structure for the inner 10 AU of a protoplanetary disk model.

**Results.** We find that the disk response to X-ray flares depends on whether the plasma temperature increases during flares and/or whether heavy metals (such as magnesium) are present in the gas phase. Under favourable conditions the outer disk dead-zone can disappear altogether, and the dead-zone located between  $0.5 < R < 2$  AU can disappear and reappear in phase with the X-ray luminosity.

**Conclusions.** X-ray flares can have a significant effect on the dead-zone structure in protoplanetary disks. Caution is required in interpreting this result as the duration of X-ray bursts is considerably shorter than the growth time of MHD turbulence due to the magnetorotational instability.

**Key words.** accretion, accretion disks – MHD - planetary systems: protoplanetary disks – stars: pre-main sequence

## 1. Introduction

Observations of young stars in a variety of star forming regions, ranging from the trapezium cluster in Orion to the Taurus–Auriga complex, have shown that protostellar disks are ubiquitous (e.g. Beckwith & Sargeant 1996; O’Dell et al. 1993; Prosser et al. 1994). These disks often show evidence for active accretion with a canonical mass flow rate onto the central star of  $\sim 10^{-8} M_{\odot} \text{ yr}^{-1}$  (e.g. Sicilia-Aguilar et al. 2004), requiring a mechanism to transport angular momentum within the disks. So far only one mechanism has been shown to work: MHD turbulence generated by the magnetorotational instability (MRI) (Balbus & Hawley 1991; Hawley & Balbus 1991).

Given that protostellar disks are cool and dense near their midplanes, there are questions about the global applicability of the MRI to these disks, as the ionisation fraction is expected to be low (Blaes & Balbus 1994; Gammie 1996). Indeed, nonlinear magnetohydrodynamic simulations of disks that include ohmic resistivity (Fleming, Stone & Hawley 2000) have indicated that for magnetic Reynolds numbers  $Re_m$  below a critical value  $Re_m^{\text{crit}}$ , tur-

bulence is not sustained and the disks return to a near-laminar state whose internal stresses are too small to explain the observed mass accretion rates onto T Tauri stars.

There have been a number of studies of the ionisation fraction in protostellar disks. Gammie (1996) first suggested that disks may have magnetically “active zones” sustained by thermal or cosmic ray ionisation, adjoining regions that are “dead-zones” where the ionisation fraction is too small to sustain MHD turbulence. Sano et al. (2000) examined this issue using a more complex chemical model that included dust grains. Glassgold et al. (1997) and Igea et al. (1999) examined the role of X-rays as a source of ionisation in protostellar disks, and highlighted doubts about whether Galactic cosmic rays could penetrate into the inner regions of protostellar disks because of the stellar wind. Fromang, Terquem & Balbus (2002) examined the influence of gas phase heavy metals and demonstrated the potential importance of charge-transfer reactions, and Semenov et al. (2004) studied disk chemistry and the ionisation fraction using a complex reaction

network drawn from the UMIST data base.

Recent observations of the X-ray emission from T Tauri stars in the Orion nebula using the Chandra observatory (COUP - Chandra Orion Ultradeep Project) have shown that in addition to providing a characteristic X-ray luminosity at a level of  $L_X \sim 10^{30}$  erg s<sup>-1</sup>, young stars emit X-ray flares whose luminosity is  $\sim 100$  times this value (e.g. Wolk et al. 2005; Favata et al. 2005). These flares typically last for less than a day, and are characterised by a sharp linear rise in luminosity, followed by an exponential decay. The typical recurrence time is about one week, and associated with the flares is a hardening of the X-ray spectrum indicating a rise in the plasma temperature in the stellar corona from  $k_B T \simeq 3$  keV to typical values of  $\simeq 7$  keV. In this paper we address the question of what effect these X-ray flares have on the ionisation fraction and structure of dead-zones in protostellar disks.

In a recent paper (Ilgner & Nelson 2006a) we compared the predictions made by a number of chemical reaction networks about the structure of dead-zones in standard  $\alpha$ -disk models. This study included an examination of the reaction scheme proposed by Oppenheimer & Dalgarno (1974), and more complex schemes drawn from the UMIST data base (Le Teuff et al. 1996). In a follow-up paper (Ilgner & Nelson 2006b) we examined the role of turbulent mixing in determining the structure of dead-zones in  $\alpha$ -disk models using chemical reaction networks drawn from (Ilgner & Nelson 2006a). In this paper we continue with our work on the ionisation structure within protoplanetary disks and examine the effect that X-ray flares have on dead-zones in  $\alpha$ -disk models using reaction networks drawn from Ilgner & Nelson (2006a).

In general we find that X-ray flares can have a fairly dramatic effect on the ionisation structure in disks, especially if the X-ray spectrum hardens during flares and/or trace quantities of heavy metals (magnesium) are present in the gas phase. Our disk models can be divided into three distinct regions: an inner region where the disk is always active due to thermal ionisation; a central region in which the dead-zone formally decreases in depth substantially or disappears altogether during X-ray flares, but which returns to being a deep dead-zone in between flares; an outer region beyond  $R = 2$  AU in which the dead-zone depth does not change in time, and which can become very thin or disappear altogether in the presence of heavy metals and an increasing plasma temperature during outbursts.

This paper is organised as follows. In section 2 we describe our modelling procedure, including the disk model, the chemical models, and our method for simulating X-ray flares. In section 3 we present the results of our models, and discuss the effects of changing the model parameters. In section 4 we discuss our results in the context of turbulent protostellar disks, and in section 5 we summarise our findings.

## 2. Model

### 2.1. Disk model

The underlying disk model considered is a standard  $\alpha$ -disk. Details are given in Ilgner & Nelson (2006a) and references therein. To recap: the disk is assumed to orbit a young solar mass star and undergo viscous evolution. We use the  $\alpha$  prescription for the viscous stress, such that the kinematic viscosity  $\nu = \alpha c_s^2 / \Omega$ , where  $c_s$  is the sound speed and  $\Omega$  is the local Keplerian angular velocity. Heating of the disk is provided by viscous dissipation alone, and cooling by radiation transport in the vertical direction. The disk structure is obtained by solving for hydrostatic and thermal equilibrium. The disk model is completely specified by the mass accretion rate,  $\dot{M}$  and the value of  $\alpha$ . In this paper we consider a single disk model with  $\dot{M} = 10^{-7} M_\odot \text{ yr}^{-1}$  and  $\alpha = 10^{-2}$ . The mass is  $0.0087 M_\odot$  between  $0.1 \leq R \leq 10$  AU.

### 2.2. Kinetic models

We have applied two kinetic models to evolve the gas-phase chemistry. Both reaction networks have been described in Ilgner & Nelson (2006a), where the models were given the labels `model11` and `model13`, respectively. For continuity, we maintain this labelling convention in this paper. To recap: `model11` refers to the kinetic model of Oppenheimer & Dalgarno (1974) while `model13` is linked to the more complex UMIST database. The underlying kinetic scheme of the Oppenheimer & Dalgarno model, involves two elements, five species, and four reactions. These species are free electrons “ $e^-$ ”, a representative molecule “ $m$ ”, a heavy metal atom “ $M$ ”, and their ionized counterparts “ $m^+$ ” and “ $M^+$ ”. We used the reference values of the rate coefficients given in Ilgner & Nelson (2006a). The UMIST kinetic model was constructed by extracting all species and reactions from a set of 174 species in the UMIST database containing the elements H, He, C, O, N, S, Si, Mg, Fe, resulting in 1965 reactions being included. A detailed description of both kinetic models is given in Ilgner & Nelson (2006a).

Apart from the ionisation rate  $\zeta$  which is discussed in a separate section below, all the other parameters are taken from Ilgner & Nelson (2006a).

### 2.3. X-ray flares

We assume that ionisation of the disk material arises because of incident X-rays that originate in the corona of the central T Tauri star. We neglect contributions from Galactic cosmic rays as it remains uncertain whether they can penetrate into inner disk regions we consider due to the stellar wind. In our previous work (Ilgner & Nelson 2006a, 2006b) we introduced the X-ray luminosity  $L_X$ , which was constant. In this work the X-ray luminosity becomes time dependent,  $L_X(t)$  because of the X-ray flares.

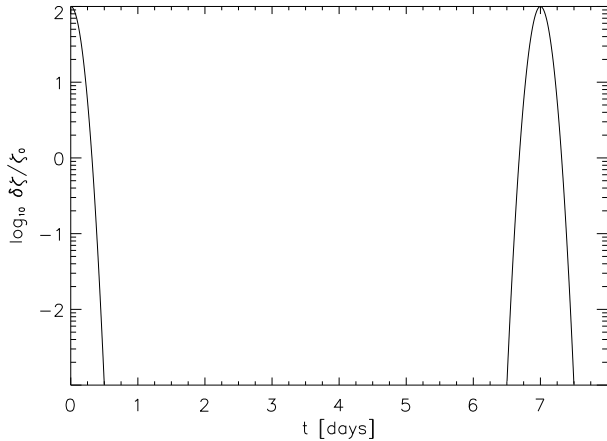


**Fig. 1.** Time sequence of the X-ray flares  $\delta\zeta/\zeta_0$ . The perturbation is periodic in time with a periodicity  $\tau_X = 7$  days while the width of a single perturbation is  $t_\sigma = 12$  hr.

We now adopt a model in which the X-ray luminosity maintains a base value,  $L_X = L_X^0$ , on top of which are superposed X-ray flares with peak luminosity  $L_X^P$ . In order to maintain the compatibility with our previous work (Ilgner & Nelson 2006a, 2006b) we use  $L_X^0 = 10^{30}$  erg/s.

We approximate the flare temporal morphology by a sequence of outbursts that arise periodically in time. The shape of a single flare is modelled by using a Gaussian profile. We note that the symmetric profile thus obtained is simpler than the observed flare morphology which is more accurately characterised as a linear rise and exponential decay, but we believe that our model captures the essentials of how X-ray flares affect the ionisation structure in the disk independently of such details. We assume that one flare occurs per week, and each outburst lasts for 24 hours. These values are similar to those observed during the Chandra Orion Ultradeep Project (COUP) as reported by Wolk et al. (2005).

For a given total X-ray luminosity  $L_X$  and plasma temperature  $k_B T$  one can calculate the ionisation rate due to X-rays at each position in the disk model. This requires an integrator along each line of sight through the disk model to the X-ray source, and our method for this is described in Ilgner & Nelson (2006a). In this paper we consider both models in which the plasma temperature remains constant, and models in which the plasma temperature varies along with the X-ray luminosity. When the plasma temperature remains constant the attenuation of the X-rays is also constant, so the temporal morphology of the X-ray luminosity and the local ionisation rate are characterised by the same mathematical function. The perturbation  $\delta\zeta$  in the local ionisation rate due to an X-ray flare is then given by the following time-dependent ionisation rate

$$\zeta(t) = \zeta_0 + \delta\zeta(t), \quad (1)$$

where

$$\delta\zeta(t) = \begin{cases} \lambda\zeta_0 \exp\left\{-\left(\frac{t-\Delta}{\sigma}\right)^2\right\} & \text{if } \Delta - t_\sigma \leq t \leq \Delta + t_\sigma \\ 0 & \text{otherwise} \end{cases} \quad (2)$$

where  $\zeta_0$  and  $\delta\zeta$  denotes the base X-ray ionisation rate and its time-dependent perturbation, respectively.  $\lambda$  is a factor that determines the amplitude of the perturbation,  $t_\sigma = 12$  hr,  $\Delta = m\tau_X$  with  $m$  as an integer, and  $\tau_X = 7$  days. Hence the characteristic width  $t_\sigma$  of a single flare is given by

$$\sigma = \frac{t_\sigma}{\sqrt{|\ln[\delta\zeta(t_\sigma)/\lambda]|}} \quad (3)$$

with  $\delta\zeta/\lambda = 10^{-5}$  for  $|t - \Delta| = t_\sigma$ . A time sequence of the modulation of  $\delta\zeta$  with  $\lambda = 100$  is shown in figure 1.

Observations indicate that the plasma temperature  $k_B T$  increases as the X-ray luminosity does during a flare. This means that we need to take account of the fact that the penetration depth also varies with time, due to the hardening of the X-ray spectrum. As we will see in section 3.3, this can have quite dramatic effects on the local ionisation rate. To model this we consider a minimum plasma temperature  $T_{\text{cool}}$  which applies when the X-ray luminosity is at its base value  $L_X^0$  and calculate the ionisation rate  $\zeta_0(R, z)$  at each position in the disk. When the X-ray luminosity has reached its peak value  $L_X^P$  we assume that the plasma temperature has reached its maximum value  $T_{\text{hot}}$ , and calculate the ionisation rate  $\zeta_P(R, z)$  at each position in the disk. The time dependent perturbation to the local ionisation rate is then given by

$$\delta\zeta(t) = \zeta_P \exp\left\{-\left(\frac{t-\Delta}{\sigma}\right)^2\right\} \quad (4)$$

if  $|t - \Delta| < t_\sigma$ , otherwise  $\delta\zeta = 0$ . In the models with varying plasma temperature, we adopt  $k_B T_{\text{cool}} = 3$  keV and  $k_B T_{\text{hot}} = 7$  keV, which are close to the observed values (Wolk et al. 2005; Favata et al. 2005)

### 3. Results

We assume  $L_X^0 = 10^{30}$  erg/s for the base value of the X-ray luminosity, in basic agreement with recent observations. During the X-ray flare the X-ray peak luminosity  $L_X^P$  is significantly larger than  $L_X^0$ . We assumed  $L_X^P = 100 \times L_X^0$  which is in line with the observed changes reported in Favata et al. (2005). The ionisation rate  $\zeta$  is then given by equations (1) and (2) with  $\lambda = 100$  if  $k_B T$  is constant, or equations (1) and (4) if  $k_B T$  varies. The time averaged value over one complete seven day cycle is  $\langle \zeta \rangle = \zeta_{\text{eff}} = 5.81 \times \zeta_0$  when  $k_B T$  has a constant value of 3 keV.

We have evolved the disk chemistry using the kinetic models `model11` and `model13` by taking the perturbation  $\delta\zeta$  of the ionisation rate due to X-ray flares into account. As in our previous studies we wish to determine which parts of the disk are sufficiently ionised for the gas to

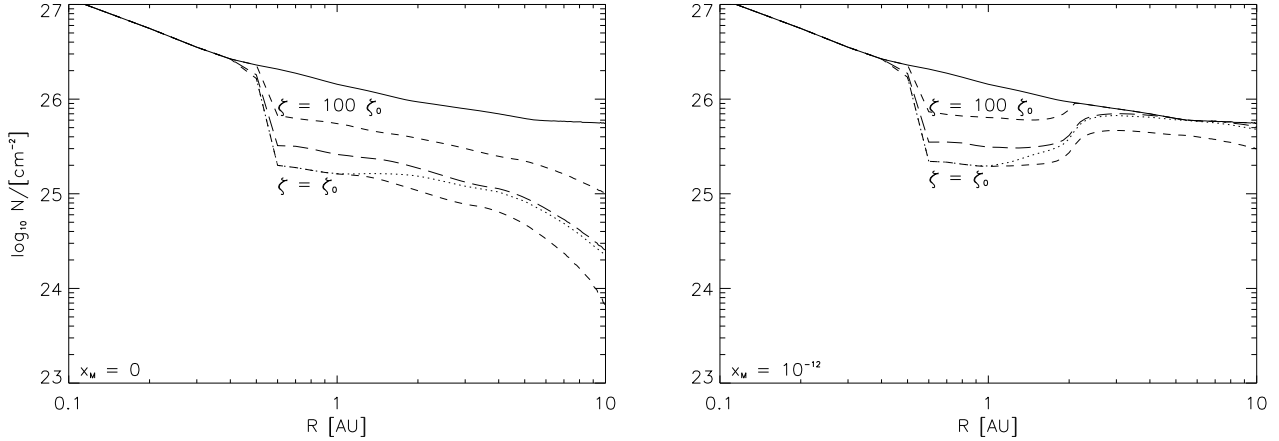


**Fig. 2.** `model11` - Column densities of the whole disk (solid line) and of the active zones (dashed and dotted lines) - corresponding to magnetic Reynolds numbers  $Re_m$  greater than 100 - for two different heavy metal abundances  $x_M$ . The left panel is for  $x_M = 0$  and the right panels is for  $x_M = 10^{-12}$ . The upper and lower dashed lines refer to simulations with constant ionisation rate  $\zeta = \zeta_0$  and  $\zeta = 100 \times \zeta_0$  while the long-dashed line refers to simulation with  $\zeta = \zeta_{\text{eff}}$ . The dotted line refers to the column density of the active zone at  $t = 10,000$  yr obtained by assuming a time-dependent ionisation rate  $\zeta(t) = \zeta_0 + \delta\zeta(t)$ . The time of the plot is at the mid-point between two X-ray flares.

be well coupled to the magnetic field, and thus able to maintain MHD turbulence, and which regions are too neutral for such turbulence to be maintained. Again, we refer to those regions as being “active” and “dead” zones respectively, with the region bordering the two being the “transition” zone. The important discriminant that determines whether the disk is active or dead is the magnetic Reynolds number,  $Re_m$ , defined by

$$Re_m = \frac{Hc_s}{\mu} \quad (5)$$

where  $H$  is the disk semi-thickness,  $c_s$  is the sound speed, and  $\mu$  is the magnetic diffusivity which is a function of the local free electron fraction. We adopt a value of  $Re_m^{\text{crit}} = 100$  in this paper, following the value used in our previous publications and Fromang et al. (2002). We are able to calculate the distribution of  $Re_m$  within our disks. Regions with  $Re_m < 100$  are deemed to be magnetically dead, and those with  $Re_m > 100$  magnetically active. The quantity  $x_{\text{crit}}[e^-]$  denotes the ionisation fraction  $x[e^-]$  along the transition zone.

Our approach to modelling the chemistry in disks with X-ray flares is as follows. First, we evolved models keeping the ionisation rate  $\zeta$  constant in time. We considered three cases with  $\zeta = \zeta_0$ ,  $\zeta = \zeta_{\text{eff}}$ , and  $\zeta = 100 \times \zeta_0$ . The kinetic equations are solved for a time interval of  $\Delta t = 100,000$  yr. Hence, the ionisation fraction  $x[e^-]$  is a function of time  $t$ , and in principle so is the location of the transition zone. However, for these models which assume a time-independent ionisation rate  $\zeta$ , the change in the vertical location of the transition zone at all cylindrical radii in the computational domain was below the grid resolution for  $t > 10,000$  yr.

Using the abundances obtained from the  $\zeta = \zeta_0$  model

at  $t = 100,000$  yr as initial abundances, we also calculated the ionisation fraction  $x[e^-]$  by considering a time-dependent ionisation rate  $\zeta = \zeta_0 + \delta\zeta$ . The kinetic equations here were solved for a time interval of  $\Delta t = 10,000$  yr. We restricted the time integration of the kinetic equations by assuming a finite maximum absolute step size  $\Delta h_{\text{max}} = 1$  hr in order to resolve the flares in time. Because of the adopted value of the perturbation  $\lambda = 100$ , models with time-independent ionisation rates  $\zeta = \zeta_0$  and  $\zeta = 100 \times \zeta_0$  represent the limiting cases for models with  $\zeta = \zeta_0 + \delta\zeta$ .

### 3.1. Snapshots at $t = 10,000$ yr with $k_B T$ constant

We begin by discussing models which have a constant plasma temperature  $k_B T = 3$  keV but varying X-ray luminosity. The effects of allowing the plasma temperature to vary are discussed in section 3.3. The discussion below relates to the disk properties at a single point in time midway between two X-ray flares. Discussion about the time dependent behaviour of the ionisation fraction and dead-zones is presented in section 3.2.

#### Oppenheimer & Dalgarno model

The results obtained for `model11` are presented in fig. 2, which shows the column density of the whole disk plotted as a function of radius using the solid line, and the column density of the active zone using either dashed lines (for which  $\zeta = \zeta_0$ ,  $\zeta = \zeta_{\text{eff}}$ , and  $\zeta = 100 \times \zeta_0$ ) or dotted lines referring to  $\zeta(t) = \zeta_0 + \delta\zeta(t)$ . The dotted line corresponds to a time which is halfway between two X-ray flares. The left panel shows cases for which the heavy metal abundance  $x_M = 0$  and the right panel shows cases with  $x_M = 10^{-12}$ .

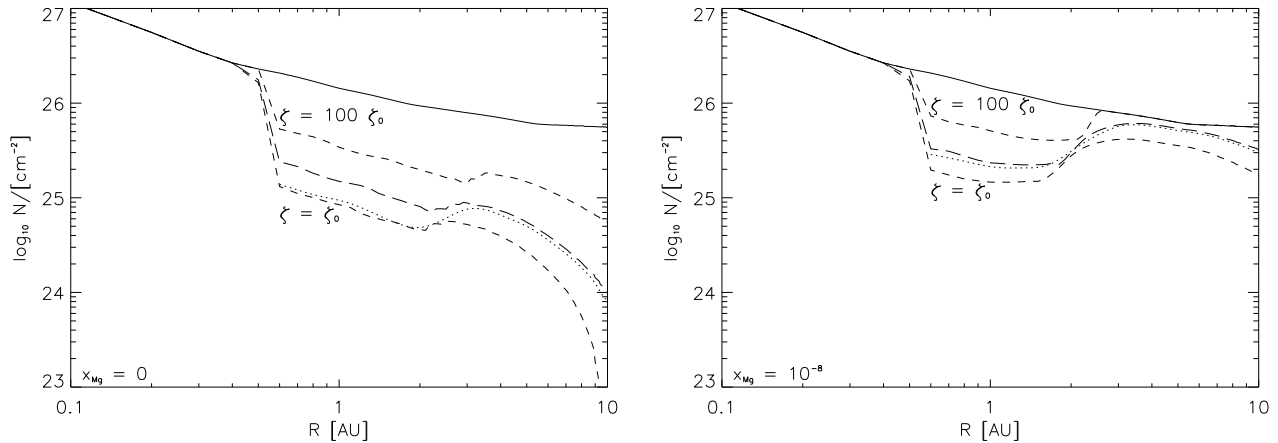


**Fig. 3.** `model3` - Column densities of the whole disk (solid line) and of the active zones (dashed and dotted lines) - referring to magnetic Reynolds numbers  $Re_m$  greater than 100 - for two different elemental abundances  $x_{Mg}$ . The left panel is for  $x_{Mg} = 0$  and the right panel is for  $x_{Mg} = 10^{-8}$ . The upper and the lower the dashed lines refer to simulations assuming a constant ionisation rate  $\zeta = \zeta_0$  and  $\zeta = 100 \times \zeta_0$ , while the long-dashed dotted line refers to simulation with  $\zeta = \zeta_{eff}$ . The dotted line shows the column density of the active zone at  $t = 10,000$  yr assuming a time-dependent ionisation rate  $\zeta(t) = \zeta_0 + \delta\zeta(t)$ . The amplitude  $\lambda$  of the perturbation  $\delta\zeta/\zeta_0$  is  $\lambda = 100$  caused by increasing the X-ray luminosity  $L_X^P = 100 \times L_X^0$  at the flare peak.

As expected, figure 2 shows that a time-independent increase in the X-ray luminosity leads to a corresponding decrease in the depth of the dead-zone (note that the disk inner regions are fully active because of thermal ionisation of potassium [Ilgner & Nelson 2006a]). Interestingly, even an increase in X-ray luminosity by a factor of 100 is insufficient to fully ionise the disk, and a dead-zone remains beyond  $R > 0.5$  AU. When we consider the X-ray flaring model, we find that the behaviour of the ionisation fraction and dead-zone depends on radial position within the disk. The region between  $0.5 < R < 1.2$  AU has the same dead-zone structure as the model with constant X-ray luminosity set at the base level  $L_X^0$ . As will be discussed in more detail later on, this is because the recombination time in this region is shorter than the period of the X-ray outburst cycle, so the disk ionisation fraction remains in phase with the X-ray luminosity. Further out in the disk beyond  $R > 2$  AU, we find that the dead-zone structure is very close to that obtained when the X-ray luminosity takes a constant value that is equal to the time-averaged value of the X-ray flaring model (i.e.  $\zeta = \zeta_{eff}$ ). This is because the recombination time is now longer than the period of the X-ray flaring, so the response of the ionisation fraction lags the instantaneous ionisation rate. Over long evolution times the disk responds to the average ionisation rate.

The right-hand panel in figure 2 shows the effect of introducing a small abundance ( $x_M = 10^{-12}$ ) of heavy metals. As described in Fromang et al. (2002) and Ilgner & Nelson (2006a), the introduction of heavy metals to the gas phase is expected to increase the free-electron fraction because of charge-transfer reactions with molecular ions. Figure 2 shows that an increase in constant

X-ray luminosity by a factor of 100 causes the dead-zone to disappear beyond 2 AU. A constant ionisation rate  $\zeta_{eff}$  corresponding to the time-average of the flaring rate leads to effective removal of the dead-zone beyond 3 AU. When we consider the X-ray flaring model we observe similar behaviour to that in the model without heavy metals. Interior to about 1 AU the dead-zone structure at the time of the snapshot is essentially the same as the one obtained when the ionisation rate has a constant value  $\zeta = \zeta_0$ . As discussed in Ilgner & Nelson (2006a), the recombination of free electrons in this region remains dominated by molecular ions even when heavy metals are present, so this result is expected. Further out in the disk the recombination becomes dominated by the heavy metal ions,  $M^+$ , and the recombination time is longer than the period of the X-ray flares. In this region the disk again responds to the time dependent X-ray flares as if the ionisation rate were equal to the time averaged value, resulting in the effective removal of the dead-zone beyond  $R \simeq 3$  AU.

### UMIST model

The results obtained for `model3` are presented in fig. 3. Here, the column density of the whole disk is plotted as a function of radius using the solid line while the dashed lines correspond to the column density of the active zone obtained for models with  $\zeta = \zeta_0$ ,  $\zeta = \zeta_{eff}$ , and  $\zeta = 100 \times \zeta_0$ . In addition, the column density of the active zone for the model employing the time dependent ionisation rate  $\zeta = \zeta_0 + \delta\zeta$  is shown by the dotted line. The left panel corresponds to models in which the elemental abundance of magnesium  $x_{Mg} = 0$ , the right panel shows results for which  $x_{Mg} = 10^{-8}$ .

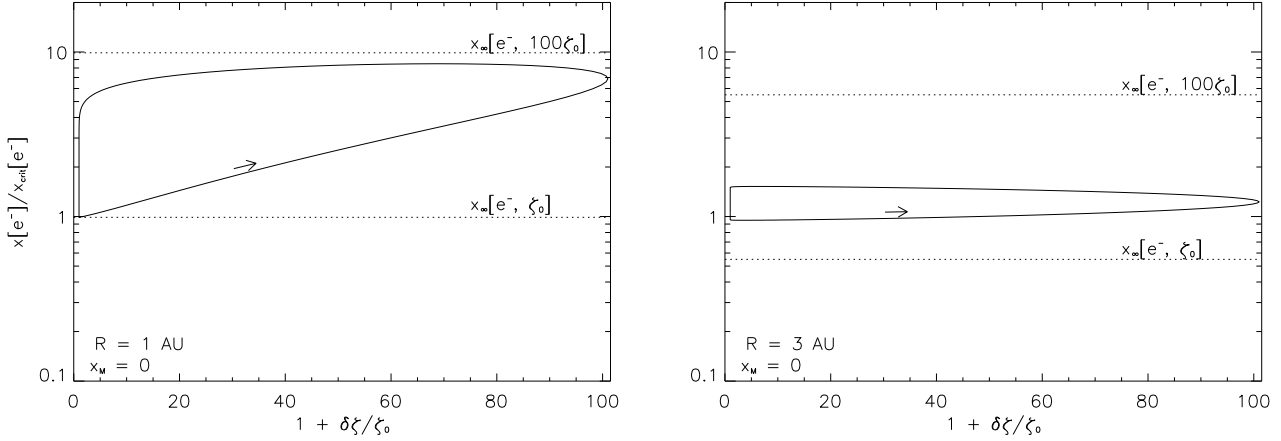


**Fig. 4. model11** - The change in the ionisation fraction  $x[e^-]/x_{\text{crit}}[e^-]$  is plotted against the relative change in the ionisation rate  $(\zeta_0 + \delta\zeta)/\zeta_0$  at different radial positions  $R$  along the transition zone assuming  $x_M = 0$ . It is a limit cycle since the orbit is closed (the arrow points forward in time). In addition, the equilibrium values  $x_\infty[e^-]$  are shown obtained for the unperturbed models with  $\zeta = \zeta_0$ , and  $\zeta = 100 \times \zeta_0$ .

Our previous work that compared the results of different chemical networks has already established that the more complex chemical models based on the UMIST data base predict deeper and more extensive dead-zones than the simpler Oppenheimer & Dalgarno models (Ilgner & Nelson 2006a). The primary reason is the larger number of molecular ions that occur in the complex chemistry, leading to a faster recombination of free electrons. Comparing figures 1 and 3 confirms this. Considering the response of **model13** to differing constant X-ray fluxes, we observe that very similar trends arise as in **model11**. For example, an increase in X-ray luminosity by a factor of 100 still leaves a substantial dead-zone beyond  $R > 0.5$  AU.

Considering **model13** with X-ray flares, we see that the dead-zone between  $0.5 < R < 2$  AU is of similar depth to that generated by the base value of the X-ray luminosity  $L_X^0$  (with associated ionisation rate  $\zeta_0$ ). This arises for similar reasons to those given when describing **model11** above: the local recombination time is shorter than the time period between X-ray flares, ensuring that the instantaneous ionisation fraction remains more or less in phase with the X-ray luminosity. Conversely, the dead-zone depth beyond  $R > 2$  AU approaches that predicted by the model whose ionisation rate  $\zeta_{\text{eff}}$  is the time average of the X-ray flaring model. This arises because the recombination time here is longer than the time period between X-ray flares, ensuring that the local ionisation fraction responds to the average X-ray luminosity rather than the instantaneous value.

The right panel shows the effect of adding an elemental abundance of magnesium  $x_{\text{Mg}} = 10^{-8}$ . For a constant X-ray luminosity increased above the base value by a factor of 100, the dead-zone disappears beyond  $R > 2$  AU. The dead-zone is predicted to be very shallow in this region by the X-ray flaring model. In both these cases, however,

a significant dead-zone remains between  $0.5 < R < 2$  AU because the dominant sources of recombination here are molecular ions rather than magnesium ions.

### 3.2. Time-dependent results beyond $t = 10,000$ yr with $k_B T$ constant

In the previous section 3.1 our analysis focused on the chemical state of the disk at a particular point in time midway between two X-ray flares after 10,000 yr of evolution. Since the ionisation rate  $\zeta(t) = \zeta_0 + \delta\zeta(t)$  changes periodically in time, so does the size of the active zone. We now focus on this periodic time dependence. We consider the time-dependent ionisation fraction at a few well-defined positions within the disk, along the transition zone defined by figures 2 and 3. We refer to the ionisation fraction at the transition zone (defined where the magnetic Reynolds number = 100) as the critical value, and denote it by  $x_{\text{crit}}[e^-]$ . Again we discuss the results of the Oppenheimer & Dalgarno model prior to the UMIST model.

#### Oppenheimer & Dalgarno model

We found that the change in  $x[e^-]$  with time  $t$  is given by a limit cycle. The limit cycle becomes apparent by plotting the ionisation fraction relative to the critical value in the transition zone  $x[e^-]/x_{\text{crit}}[e^-]$  against the change in the ionisation rate  $(\zeta_0 + \delta\zeta)/\zeta_0$ . The ionisation fraction repeats with a periodicity of  $\tau_X$  resulting in a closed orbit. Examples of limit cycles obtained for **model11** in the absence of heavy metals are shown in figure 4; note that the arrow points forward in time such that the cycle is traced in an anticlockwise direction. The left hand panel shows the variation of  $x[e^-]$  at  $R = 1$  AU for **model11**. The limit cycles obtained at  $R \leq 1$  AU with  $x_M = 10^{-12}$  are quite similar to those obtained with  $x_M = 0$  since the

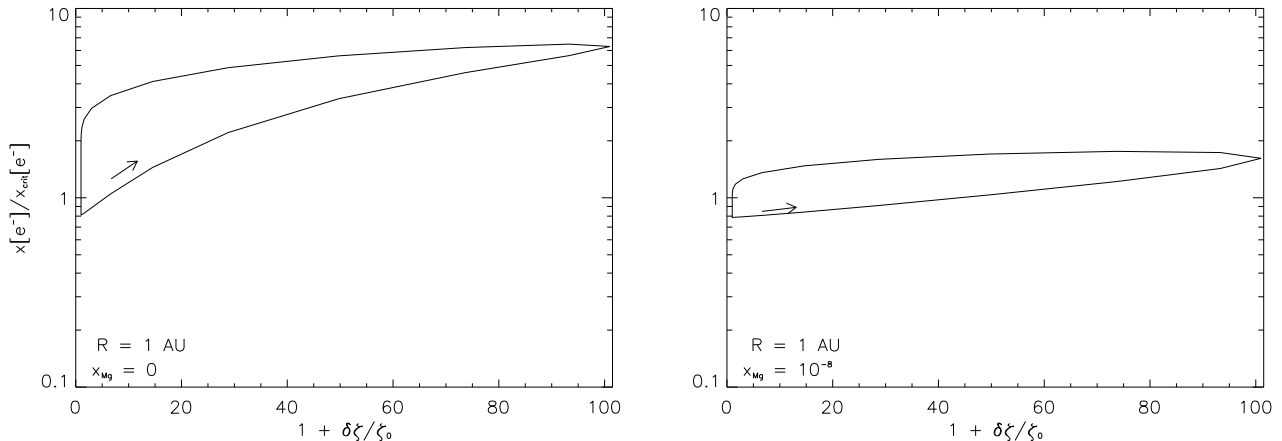


**Fig. 5. model3** - The change in the ionisation fraction  $x[e^-]/x_{\text{crit}}[e^-]$  is plotted against the relative change in the ionisation rate  $(\zeta_0 + \delta\zeta)/\zeta_0$  near the transition zone at  $R = 1$  AU for different elemental abundances  $x_{\text{Mg}}$ . The left panel is for  $x_{\text{Mg}} = 0$  and the right panel is for  $x_{\text{Mg}} = 10^{-8}$ . It is a limit cycle since the orbit is closed (the arrow points forward in time). Note that  $x[e^-]/x_{\text{crit}}[e^-]$  is slightly less than unity when  $\zeta = \zeta_0$  because the position of the transition zone does not coincide precisely with a grid cell in this model.

molecular ion still dominates the recombination of free electrons there. At locations where metal ions dominate when they are included, such as at 3 AU (as shown in the right panel of figure 4) the change in the ionisation fraction  $x[e^-]$  across the limit cycle is tiny and would appear as a straight line when using the same scale of figure 4. The results of **model11** at 3 AU without heavy metals shows a modest rise in ionisation fraction during the cycle, as shown by the right panel of figure 4.

The time required for the system to establish a limit cycle varies depending on the local position along the transition zone, but to within an accuracy of 0.1% limit cycles were achieved throughout the disk for **model11**, with and without heavy metals.

We differentiate between limit cycles for which the change in ionisation fraction  $x[e^-]$  lags substantially behind the corresponding ionisation rate  $\zeta(t)$ , and those for which  $x[e^-]$  does not. The former behaviour is illustrated by the right panel of figure 4 where the value of  $x[e^-]$  continues to rise during the rise *and* fall of the perturbed ionisation rate  $(\zeta_0 + \delta\zeta)/\zeta_0$  during an X-ray flare. This phenomenon occurs only in those regions where the recombination time is sufficiently long that the instantaneous recombination rate is smaller than the instantaneous perturbed ionisation rate for the duration of the flare. Once the flare has died away then the ionisation fraction slowly decreases back down to its original value, just in time for the next flare to begin. This slow decrease in  $x[e^-]$  arises because the recombination time is longer than the time period between X-ray flares.

The left panel of figure 4 shows an example where the changes in ionisation fraction are more in phase with the perturbation to the ionisation rate. This occurs in regions where the recombination time becomes short compared to the perturbed ionisation rate during a flare. The on-

set of an X-ray flare leads to a quite dramatic rise in the ionisation fraction at the transition zone. As the flare reaches its peak and begins to subside, the recombination rate starts to exceed the ionisation rate and the ionisation fraction decreases while the flare subsides. At the point where the flare ends the perturbation to  $x[e^-]$  has dropped from a peak value of  $x[e^-] \simeq 8x_{\text{crit}}[e^-]$  down to  $x[e^-] \simeq 4x_{\text{crit}}[e^-]$ . Once the flare has subsided completely the ionisation fraction drops to the value corresponding to the steady state obtained when the X-ray luminosity has its base value (with associated ionisation rate  $\zeta_0$ ). This final drop in the ionisation fraction to the critical value  $x[e^-]_{\text{crit}}$  at the transition zone occurs because the recombination time is shorter than the time period between X-ray flares.

Figure 4 also shows that the duration of the X-ray flares is too short to reach the ionisation fraction obtained for **model11** with a constant ionisation rate  $\zeta = 100\zeta_0$ . Indeed we found that for the unperturbed models the transition from state  $x_\infty[e^-; \zeta_0]$  to  $x_\infty[e^-; 100 \times \zeta_0]$  occurs on time scales between 1 day (at  $R = 1$  AU) and 90 days (at  $R = 10$  AU), where  $x_\infty$  denotes the steady fractional abundance.

### UMIST model

We now continue by discussing the time dependent evolution of the ionisation fraction  $x[e^-]$  obtained for **model13** at positions in the immediate vicinity of the transition zone for times beyond 10,000 yr. Once again we found limit cycle behaviour throughout the disk, but in order to obtain periodic orbits beyond radii  $R > 2$  AU we had to evolve the disk slightly beyond 10,000 yr (since a steady-state had not been reached by 10,000 yr). Figure 5 shows examples of the limit cycles obtained at  $R = 1$  AU in the absence of magnesium (left panel) and with an abundance of magne-

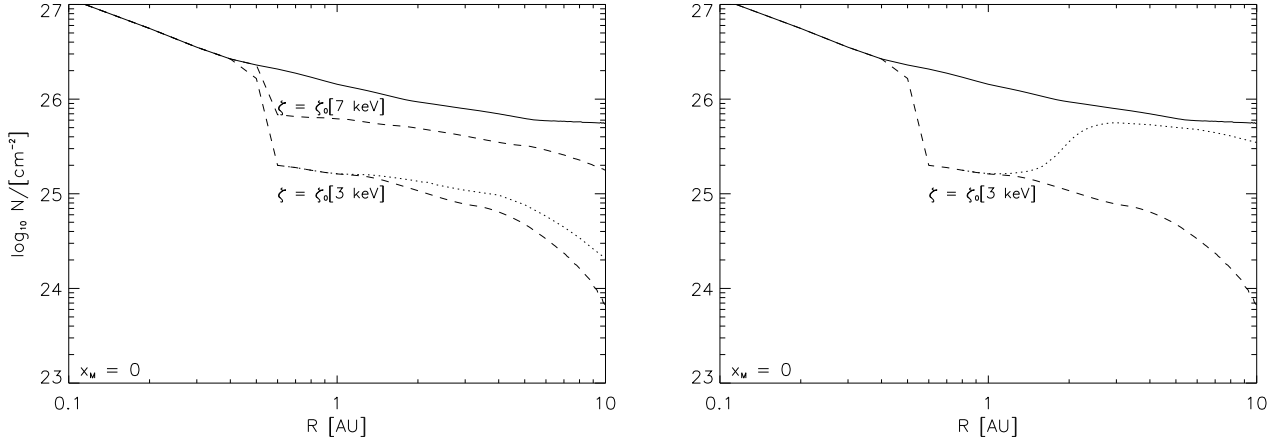


**Fig. 6.** - `model1` - Column densities of the whole disk (solid line) and of the active zones (dashed and dotted lines) - referring to magnetic Reynolds numbers  $Re_m > 100$  - for  $x_M = 0$ . The dashed lines refer to simulations obtained by assuming unchanging ionisation rates  $\zeta = \zeta_0$  for different plasma temperatures.

left panel: The dotted line refers to the column density of the active zone at  $t = 10,000$  yr obtained by assuming a time-dependent ionisation rate caused by periodic variation of the plasma temperature between  $k_B T_{cool} = 3$  keV and  $k_B T_{hot} = 7$  keV.

right panel: The dotted line refers to the column density of the active zone at  $t = 10,000$  yr obtained by assuming a time-dependent ionisation rate  $\zeta(t)$  caused by both the X-ray luminosity and the plasma temperature increasing during flares. The disk becomes entirely active when the X-ray luminosity is increased by a factor of 100 and the plasma temperature is maintained at a constant value of  $k_B T = 7$  keV.

sium  $x_{Mg} = 10^{-8}$  (right panel). For that region, metals do not have a dramatic effect on the ionisation fraction  $x[e^-]$  because molecular ions still dominate the recombination process of free electrons (see Ilgner & Nelson 2006a). It is clear that in both cases the free electron fraction remains close to being in phase with the changing X-ray luminosity, with  $x[e^-]$  increasing as  $(\zeta_0 + \delta\zeta)/\zeta_0$  increases, and decreasing as  $(\zeta_0 + \delta\zeta)/\zeta_0$  does. Here the recombination rate becomes larger than the ionisation rate immediately after the peak of the X-ray flare, causing the ionisation fraction to decrease as the flare intensity diminishes. The ionisation fraction returns to the value obtained for a steady X-ray flux with ionisation rate  $\zeta_0$  shortly after the flare finishes, and remains at this value until the onset of the next flare. As was the case with the Oppenheimer & Dalgarno model, this fall of the ionisation fraction to the base value occurs because the recombination time is shorter than the time period between X-ray flares.

For regions beyond  $R \geq 2$  AU we evolved the chemistry for times beyond  $t = 10,000$  yr until limit cycle behaviour was obtained. These limit cycles were very similar to those shown in the right panel of figure 4, having similar amplitudes for the case without magnesium, and very small amplitudes when magnesium was included with  $x_{Mg} = 10^{-8}$ .

### 3.3. Results with varying plasma temperature $k_B T$

In the preceding sections we discussed the effects of changing the X-ray luminosity during a flare on the ionisation

structure of a disk model, while keeping the plasma temperature constant. Observations, however, indicate that the plasma temperature  $k_B T$  increases during flaring activity, resulting in the hardening of the X-ray spectrum and an increased ability of X-ray photons to penetrate into the disk (Wolk et al. 2005). Modelling of X-ray sources often requires a two-phase emission model (Mewe, Kaastra & Liedahl 1995), corresponding to two different temperatures for the cooler and hotter plasma components of the corona. Observations indicate that the cooler component remains essentially unaffected during a flare, while the hotter component increases significantly. In our model we assume that  $k_B T_{cool} = 3$  keV and  $k_B T_{hot} = 7$  keV, in close agreement with observations.

The requirement that we temporally resolve the X-ray flares while solving the kinetic equations for the chemistry means that a maximum time-step of 1 hour was adopted. This causes the calculations to become very expensive computationally, such that for the UMIST model `model13` a calculation lasting for 10,000 yr requires a run time of approximately three weeks for each grid-point of the disk model. As a consequence we have been forced to only consider the Oppenheimer & Dalgarno model `model11` in the following sections. We simply note at this point that `model11` tends to generate thinner dead-zones than `model13`, such that the results described below represent an optimistic view of which fraction of the disk can sustain MHD turbulence. We note further, however, that similar trends in the results are obtained with `model11` and `model13` when varying physical parameters, such that



`model1` gives a reasonable picture of how the ionisation fraction obtained using the more complex `model3` responds to changes in ionisation rate etc.

We begin by presenting the results of a model in which we consider the effects of increasing the plasma temperature during an X-ray flare, keeping the X-ray luminosity  $L_X$  constant. This allows us to isolate the effects of the hardening of the X-ray spectrum due to the rising plasma temperature. We then consider a model for which both the plasma temperature and the X-ray luminosity increase during flaring activity.

### Snapshot at 10,000 yr with $L_X$ constant and $k_B T$ varying

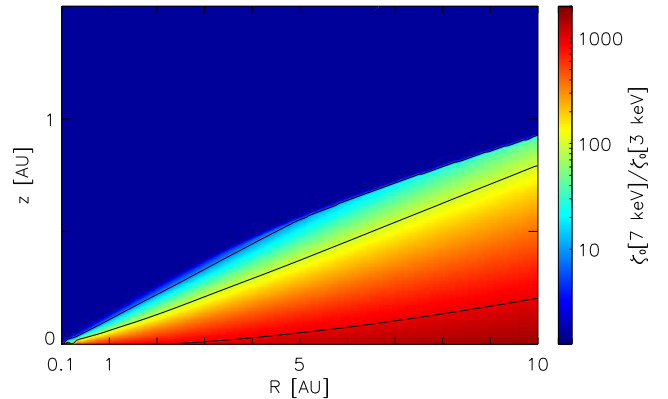
The results for this calculation are shown in the left panel of figure 6 which shows the column density of the whole disk plotted as a function of radius using the solid line. The dashed lines show the column density of the active zone for two calculations that assumed constant plasma temperatures of  $k_B T = 3$  keV and  $k_B T = 7$  keV, respectively, and the dotted line corresponds to the model whose plasma temperature rose to  $k_B T = 7$  keV during flares only without an accompanying increase in  $L_X$  above  $10^{30}$  erg s $^{-1}$ . Note that these figures refer to `model1` with no heavy metal included.

Figure 7 shows contours of the relative ionisation rate when the plasma temperature is raised from  $k_B T = 3$  to 7 keV. The change in  $\zeta$  is dramatic in the deeper, more shielded regions simply because of increased penetration induced by the hardening of the X-ray spectrum. Near the disk surface the change is only slight, but in the interior the local ionisation rate can increase by more than a factor of 1000.

The upper dashed line in the left panel of figure 6 shows that having a constantly increased value of  $k_B T = 7$  keV significantly reduces the depth of the dead-zone throughout the disk. The dotted line, however, shows that at a point in time midway between two peaks in the plasma temperature, the dead-zone is unaffected interior to  $R < 1.2$  AU because of the fast recombination time there. Beyond  $R > 2$  AU the dead-zone is a little thinner where the recombination time is longer than the period between increases in plasma temperature, corresponding closely to that which would be obtained by exposure to the time averaged value of the time dependent ionisation rate.

### Results with $L_X$ and $k_B T$ varying

A snapshot of the results obtained after 10,000 yr when the X-ray luminosity *and* the plasma temperature increase during a flare is shown in the right panel of figure 6. The solid line gives the column density of the whole disk, and the dashed line gives the column density of the active zone obtained when the X-ray luminosity is constant and takes its base value  $L_X^0$ . The disk becomes active everywhere if we take a constant ionisation rate with  $L_X = 100L_X^0$  and  $k_B T = 7$  keV. The dotted line corresponds to the model for which the plasma temperature and X-ray luminosity increase during a flare. Note that these models are



**Fig. 7.** The ratio of the effective X-ray ionisation rates  $\zeta_{0.7 \text{ keV}} / \zeta_{0.3 \text{ keV}}$ .  $\zeta_{0.3 \text{ keV}}$  and  $\zeta_{0.7 \text{ keV}}$  refer to local ionisation rates for plasma temperatures  $k_B T = 3$  keV and  $k_B T = 7$  keV, respectively. The disk parameters are  $\alpha = 10^{-2}$  and  $\dot{M} = 10^{-7} M_\odot \text{yr}^{-1}$ . The contour lines refer to values of  $\zeta_{0.7 \text{ keV}} / \zeta_{0.3 \text{ keV}}$ : 10,  $10^2$ , and  $10^3$ .

`model1` in the absence of heavy metals, and the snapshot is taken at a time that is midway between two X-ray flares. In the inner regions  $R < 1.2$  AU the dead-zone size is again unaffected by the flares between outbursts because of the rapid recombination time there. Beyond  $R > 2$  AU, however, the dead-zone depth has been decreased substantially such that the column density of the active zone includes approximately 80 % of the matter in the region between  $R = 3 - 7$  AU. Although not plotted in figure 6, the addition of heavy metals with  $x_M = 10^{-12}$  causes the dead zone to disappear completely beyond  $R > 2$  AU, although a dead-zone ranging between  $0.4 < R < 2$  AU remains.

We now consider the time dependent evolution after 10,000 yr has elapsed. The evolution of the ionisation fraction at the disk midplane (and not at the transition zone as in previous similar figures) as a function of the perturbed ionisation rate is shown in figure 8 at radii  $R = 1$  AU and  $R = 5$  AU for `model1` in the absence of heavy metals. The first thing to note is the large perturbation to the ionisation rate experienced at the disk midplane, as illustrated by the range of values for  $(\zeta_0 + \delta\zeta) / \zeta_0$ . Second, the ionisation fraction, relative to the critical value  $x_{\text{crit}} [e^-]$ , at the midplane located at  $R = 1$  rises from 0.1 (implying the region is dead) to a value of  $\approx 2$  (implying that the region is active). Thus, the inner regions of the disk show the limit cycle behaviour, and oscillate from having a dead-zone near the midplane to having an active zone there which lasts for a duration slightly longer than half the flare (i.e. about 12 hours). This region remains formally “dead” for the other six and a half days during the X-ray flaring cycle.

Although at first sight this would appear to indicate that the stress associated with MHD turbulence in a pro-

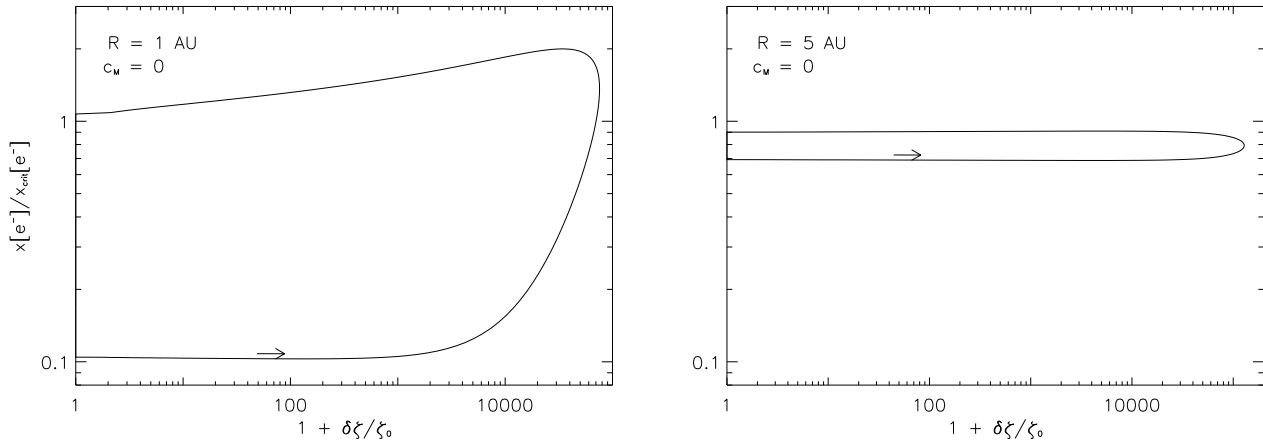


**Fig. 8. model11** - The change in the ionisation fraction  $x[e^-]/x_{\text{crit}}[e^-]$  is plotted against the relative change in the ionisation rate  $(\zeta_0 + \delta\zeta)/\zeta_0$  at different radial positions  $R$  with  $z/R = 0$  (midplane).  $x_{\text{crit}}[e^-]$  denotes the ionisation fraction at the transition layer. Each graph describes a limit cycle since the orbit is closed (the arrow points forward in time). The perturbation  $\delta\zeta/\zeta_0$  in the ionisation rate is based on the assumption that both the X-ray peak luminosity  $L_X^P = 100 \times L_X^0$  and the temperature of the hot plasma component  $k_B T_{\text{hot}} = 7$  keV at the flare peaks.

topplanetary disk would be episodic, leading to episodic mass accretion, it is important to bear in mind that the local growth rate for the MRI is approximately the local dynamical time (Balbus & Hawley 1991), which is longer than 12 hours in the regions beyond 0.5 AU. It is therefore unclear whether such a region of the disk could maintain fully developed turbulence and an associated dynamo when perturbed by X-ray flares of short duration. This issue is discussed below.

The right panel of figure 8 shows the evolution of  $x[e^-]/x_{\text{crit}}[e^-]$  versus the perturbation to the local ionisation rate  $(\zeta_0 + \delta\zeta)/\zeta_0$  at the disk midplane at  $R = 5$  AU. Here it is clear that limit cycle behaviour is again obtained, with the ionisation fraction showing a closed orbit. In this part of the disk, there remains a thin dead-zone throughout the cycle when heavy metals are not present. The addition of heavy metals with abundance  $x_{\text{Mg}} = 10^{-12}$  renders the disk fully active in this region for the whole duration of the X-ray cycle when both the luminosity and plasma temperature vary.

#### 4. Discussion

In this paper we have calculated the response of the ionisation fraction in a standard  $\alpha$ -disk model to the presence of X-ray flares originating in the corona of the central T Tauri star. For comparison purposes we have examined how the disk responds to constantly acting X-ray induced ionisation rates  $\zeta_0$  (the base ionisation rate),  $\zeta_{\text{eff}}$  (the time averaged ionisation rate), and  $100\zeta_0$  (which is the peak ionisation rate during a flare). We have considered cases where the plasma temperature retains a constant value of  $k_B T = 3$  keV during the flare cycle, and cases where the plasma temperature increases from 3 keV to 7 keV at the peak of a flare. Broadly speaking, the behaviour of the

dead-zones in our disk model can be divided into three basic regions when subject to X-ray flares:

(i). An inner region  $R < 0.5$  AU where the disk is entirely active due to thermal ionisation of potassium throughout the calculations.

(ii). A central region  $0.5 < R < 2$  AU where the disk exhibits a significant dead-zone between outbursts, but whose dead-zone can be significantly diminished or be removed altogether near the peak of an outburst. This behaviour occurs because of the short recombination time here, even when heavy metals are included in the gas phase due to the recombination being dominated by molecular ions. This causes the ionisation fraction to remain close to being in-phase with the ionisation rate during and between flares. Our calculations indicate that allowing the plasma temperature to increase to  $k_B T = 7$  keV during X-ray flares can cause the magnetic Reynolds number to exceed 100 for about 12 hours after the peak of the flare, such that the dead-zone here is formally removed for that time.

(iii). An outer region  $R > 2$  AU where the dead-zone size and depth does not change significantly during the flaring cycle. Here the dead-zone size corresponds closely to that obtained by the time-averaged X-ray flux, because the recombination time exceeds the time period of the X-ray outburst cycle. The depth of the dead-zone size in this region is significantly diminished if heavy metals are present in the gas phase *or* the plasma temperature increases during flares. The dead-zone may disappear altogether if metals are present *and* the plasma temperature increases during flares. In the absence of heavy metals and an increasing plasma temperature, the time averaged ionisation rate during a flare cycle  $\approx 5.8\zeta_0$ , and a significant dead-zone remains.

Given this disk structure consisting of an inner region without a dead-zone, a central region whose dead-zone can change significantly or be removed during parts of the X-ray flaring cycle, and an outer region which may maintain a thin dead-zone of almost constant depth, it is interesting to speculate how MHD turbulence in the system will evolve in time. Clearly the innermost regions can sustain MHD turbulence continuously, as can the magnetically active component of the outer disk. The behaviour of the central region whose magnetic Reynolds number varies significantly throughout the X-ray flaring cycle is less clear. In this region the dead-zone remains deep for six and a half days and is formally reduced in size or removed for only about 12 hours.

In the ideal MHD limit the fastest growing mode of the MRI has wave number  $k_{\max}$  defined by  $k_{\max}v_A \approx \Omega$ , where  $v_A$  is the Alfvén speed and  $\Omega$  is the local Keplerian angular velocity. The growth rate associated with this mode is  $\approx \Omega$  (actually closer to  $0.75\Omega$  [Balbus & Hawley 1991]). Ohmic resistivity strongly affects the growth of linear modes with wave number  $k$  when the associated diffusion rate  $k^2\eta$  exceeds the linear growth rate. Comparing these rates for the fastest growing mode provides a condition for the effects of resistivity to dominate over the growth of the mode due to the MRI:

$$k_{\max}^2\eta > k_{\max}v_A \quad (6)$$

which yields the condition

$$\frac{v_A^2}{\eta\Omega} < 1. \quad (7)$$

Equation (7) is often used to provide an alternative definition of the magnetic Reynolds number  $Re'_m = v_A^2/(\eta\Omega)$  (e.g. Sano, Inutsuka & Miyama 1998) which is related to the definition used in this paper by

$$Re_m = \frac{\beta}{2}Re'_m. \quad (8)$$

where  $\beta = 2c_s^2/v_A^2 = P_{\text{gas}}/P_{\text{mag}}$ .  $P_{\text{gas}}$  and  $P_{\text{mag}}$  are the gas and magnetic pressure. Thus a value of  $Re_m = 100$  corresponds to a value of  $Re'_m = 1$  when  $\beta = 200$ , such that resistivity dominates over the growth of the fastest growing mode for values of  $Re_m$  and  $Re'_m$  smaller than these.

For the purpose of illustration, let us consider a situation where  $\beta = 200$  in the central regions of our disk near the location  $R = 0.5$  AU, where the inverse of the Keplerian angular velocity  $\Omega^{-1} = 20.5$  days. An X-ray flare arises, raising the value of  $Re_m > 100$  for 12 hours, allowing exponential growth of the fastest growing mode for this time such that an amplification of  $\approx 2.5\%$  occurs. Given our definition of  $Re_m$  it is clear that any field amplification that occurred while  $Re_m > 100$  is diffused away within the next 12 hours after  $Re_m$  drops below 100, and the growth of this mode is unable to amplify the field or drive the disk toward a turbulent state. The situation can in principle be different for longer wavelength modes.

Consider the longest wavelength mode that can fit within the disk vertical extent with wavelength  $\lambda = 2H$ , and associated wavenumber  $k_{\min} = \pi/H$ . The wave number associated with the fastest growing mode has  $k_{\max} = 10/H$  if  $\beta = 200$ , such that  $k_{\max}/k_{\min} \approx 3$ . The diffusion time associated with the longest wavelength mode is an order of magnitude longer than for the fastest growing mode (whereas the growth rate is approximately half of the maximum value). Thus any field amplification that occurs during the 12 hours when  $Re_m > 100$  is diffused away over the next  $\approx 5$  days. This suggests that an X-ray flaring cycle with a periodicity of less than five days could in principle lead to gradual field amplification over successive cycles. The question of whether fully developed turbulence can arise in such a scenario is unclear, and can only be addressed by means of non linear simulations that explicitly account for periodic rises in the ionisation rates due to X-ray flaring and electron recombination.

The calculations presented in this paper consider only gas-phase chemistry, and ignore the effects of dust. As such they are relevant to a stage in protoplanetary disk evolution when substantial grain growth has occurred and a dense dust layer has settled near the midplane. It is well known, however, that small dust grains are able to sweep up free electrons and substantially reduce the ionisation fraction (e.g. Sano et al. 2000; Ilgner & Nelson 2006a), and the assumption of gas-phase chemistry is only really valid when the abundance of dust grains has been depleted by a factor of between  $10^{-4} - 10^{-8}$  below the canonical concentration of  $10^{-12}$  (Ilgner & Nelson 2006a). An open question that we have not addressed is what happens to species that are adsorbed onto the surfaces of small grains during X-ray flares, and in particular what happens to the adsorbed electrons. Najita et al. (2001) considered the effect of nonthermal desorption of grain mantles due to X-rays, but did not include the desorption of electrons into the gas phase. We speculate that if grain mantles and electrons are desorbed into the gas phase during X-ray flares, and are adsorbed back onto the grains during the time between flares, then the behaviour of the dead-zones throughout the disk will be similar to that already observed in the central regions between  $0.5 < R < 2$  AU. This is because electrons adsorb onto grains very rapidly throughout the disk, such that the time scale of which electrons will be removed from the gas phase is shorter than the time between flares. An analysis of this issue will be presented in a future publication.

## 5. Summary

We have considered the effect of X-ray flares on the ionisation fraction and dead-zone structure in protoplanetary disks. These flares can have a significant effect on dead-zones if much of the submicron sized dust in the disk has undergone grain growth and settled toward the midplane, if the plasma temperature increases significantly during X-ray flares, and/or trace quantities of heavy metals (magnesium) are present in the gas phase.

Questions remain, however, about the disk response in regions where the dead-zone is removed during an X-ray flare, but reappears during the low state. In particular it is not clear that MHD turbulence can be generated there as the growth time of the MRI is longer than the duration of the flares. This issue needs to be addressed using non linear simulations that take account of the time dependent ionisation rates induced by X-ray flares.

*Acknowledgements.* This research was supported by the European Community's Research Training Networks Programme under contract HPRN-CT-2002-00308, "PLANETS". The calculations presented here were performed using the QMUL HPC facility purchased under the SRIF initiative. We wish to thank Eric Feigelson for information provided concerning X-ray flares during the early stages of this project.

## References

- Balbus, S. A., Hawley, J. F., 1991, ApJ, **376**, 214  
 Beckwith, S., Sargent, A., 1996, Nature, **383**, 139  
 Blaes, O., Balbus, S., 1994, ApJ, **421**, 163  
 Favata, F., Flaccomio, E., Reale, F., Micela, G., Sciortino, Shang, H., Stassub, K., Feigelson. E. D., 2005, ApJS, **160**, 469  
 Fleming, T., Stone, J., Hawley, J., 2000, ApJ, **530**, 464  
 Fromang, S., Terquem, C., Balbus, S., 2002, MNRAS, **329**, 18  
 Gammie, C., 1996, ApJ, **457**, 355  
 Glassgold, A., Najita, J., Igea, J., 1997, ApJ, **480**, 344  
 Hawley, J.F., Balbus, S.A., 1991, ApJ, **376**, 223  
 Igea, J., Glassgold, A., 1999, ApJ, **518**, 848  
 Ilgner, M., Nelson, R., 2006a, A&A, **445**, 205  
 Ilgner, M., Nelson, R., 2006b, A&A, **445**, 223  
 Le Teuff, Y., Millar, T., Markwick, A., 2000, A&A, **146**, 157  
 Mewe, R., Kaastra, J.S., Liedahl, D.A., 1995, Legacy 6, 16  
 Najita, J., Bergin, T., Ullom, J., 2001, ApJ, **561**, 880  
 O'Dell, C.R., Wen, Z., Hu, X., 1993, ApJ, **410**, 696  
 Oppenheimer, M., Dalgarno, A., 1974, ApJ, **192**, 29  
 Prosser, C., Stauffer, J., Hartmann, L., Soderblom, D., Jones, B., Werner, M., McCaughrean, M., 1994, ApJ, **421**, 517  
 Sano, T., Miyama, S., Umebayashi, T., Nakano, T., 2000, ApJ, **543**, 486  
 Semenov, D., Wiebe, D., Henning, Th., 2004, A&A, **417**, 93  
 Sicilia-Aguilar, A., Hartmann, L., Briceno, C., Muzerolle, J., Calvet, N., 2004, AJ, **128**, 805  
 Wolk, S.J., Harnden, F.R., Flaccomio, E., Micela, G., Favata, F., Shang, H., Feigelson. E. D., 2005, ApJS, **160**, 423